



Future projection of droughts over major river basins in Southern Africa at specific global warming levels

Babatunde J. Abiodun¹ · Nokwethaba Makhanya¹ · Brilliant Petja^{2,3} · Abayomi A. Abatan⁴ · Philip G. Oguntunde⁵

Received: 1 October 2018 / Accepted: 20 October 2018
© Springer-Verlag GmbH Austria, part of Springer Nature 2018

Abstract

Reliable drought projections are crucial for the effective managements of future drought risk. Most of the existing drought projections over Southern Africa are based on precipitation alone, neglecting the influence of potential evapotranspiration (PET). The present study shows that inclusion of PET may alter the magnitude and robustness of the drought projections. The study used two drought indices to project potential impacts of global warming on Southern African droughts, focusing on four major river basins. One of the drought indices (SPEI: Standardized Precipitation Evapotranspiration Index) is obtained from climate water balance (i.e. precipitation minus potential evapotranspiration) while the other (SPI: Standardized Precipitation Evapotranspiration Index) is calculated from precipitation alone. For the projections, we analyzed multi-model regional climate simulations from the Coordinated Regional Climate Downscaling Experiment (CORDEX) at four specific global warming levels (GWLs) (i.e., 1.5 °C, 2.0 °C, 2.5 °C, and 3.0 °C) above the pre-industrial level and used the self-organizing maps to classify the drought projections into groups based on their similarities. Our results show that the CORDEX simulations give a realistic representation of all the necessary climate variables for quantifying droughts over Southern Africa. The simulations project a robust increase in SPEI drought intensity and frequency over Southern Africa and indicate that the magnitude of the projection increases with increasing GWLs, especially over the various river basins. In contrast, they project a non-significant change in SPI droughts at all the GWLs. The majority of the simulations clearly distinguish between the projected SPEI and SPI drought patterns, and the distinction becomes clearer with increasing GWLs. Hence, using precipitation alone for drought projection over Southern Africa may underestimate the magnitude and robustness of the projections. This study has application in mitigating climate change impacts on drought risk over Southern African river basins in the future.

1 Introduction

Drought poses a challenge to socio-economic activities in Southern African countries, where agriculture and industry depend on water from river basins. Drought depletes soil moisture and makes the soil unsuitable for crop and livestock farming,

thereby leading to food insecurity (Blench and Marriage 1999; Dai 2011; Mishra and Singh 2010). In Southern Africa, hydrological droughts often induce widespread famine, disease outbreaks, and loss of life (Calow et al. 2010; Masih et al., 2014). For example, in 1991–1992, a drought triggered widespread crop destruction in the Limpopo river basin and caused huge agricultural and economic losses in the riparian countries (Ujeneza and Abiodun 2015; Mniki 2009). In Zimbabwe, the drought reduced agricultural production by 45%, manufacturing output by 9.3%, and the gross domestic product (GDP) by 11%. In Mozambique, about US\$ 200M was spent on food aid relief for 1.3 million people who faced starvation. And, in South Africa, the drought lowered the national GDP by 1.8% (about US\$ 500M) and caused an outbreak of cholera (Davis and Vincent 2017). More recently (2015–2017), in the Western Cape (South Africa), a severe drought reduced the dam levels to about 20% and stressed the socio-economic activities of about 3.5 million people living in Cape Town (Botai et al. 2017), the most popular tourist city in Africa (StatsSA, 2012). There are indications that ongoing climate change may enhance the

✉ Babatunde J. Abiodun
babiodun@csag.uct.ac.za

¹ Climate System Analysis Group, Department of Environmental and Geographical Science, University of Cape Town, Cape Town, South Africa

² Water Research Commission, Pretoria, South Africa

³ Risk and Vulnerability Science Centre, University of Limpopo, Polokwane, South Africa

⁴ School of Geosciences, University of Edinburgh, Edinburgh, UK

⁵ Department of Agricultural and Environmental Engineering, Federal University of Technology, Akure, Nigeria

intensity and frequency of Southern Africa droughts (Kusangaya et al. 2014; Zhao and Dai 2015). Meanwhile, the high-level dependence on rain-fed agriculture makes Southern Africa one of the most susceptible regions to climate change (Dai 2011; IPCC, 2007). Hence, there is keen interest in mitigating climate change impacts on socio-economic activities on subcontinent. However, the success of any mitigation strategies depends on reliable and robust climate information.

As part of global efforts to mitigate climate change impacts, the United Nations Framework Convention on Climate Change (UNFCCC) has reached an agreement, called the Paris Agreement (Hulme 2016; Schleussner et al. 2016; Rogelj et al. 2016). The Paris Agreement aims to limit the global mean temperature to 1.5 °C and 2.0 °C above pre-industrial levels (Hulme 2016; Schleussner et al. 2016; Rogelj et al. 2016). Hulme (2016) suggested that, given that the GWL of 1 °C above pre-industrial levels has already been reached, studies should focus on investigating the impacts of a further 0.5 °C increase with respect to the present-day, and quantify the difference in climatic impacts of keeping the global warming to 1.5 °C as opposed to 2 °C. Several studies have discussed the consequences of achieving this target on global climate (e.g., Gosling et al., 2017), as well as on regional climates (Donnelly et al. 2017; Karmalkar and Bradley 2017; Schleussner et al. 2016), but there is no agreement in their findings. For instance, while Schleussner et al. (2016) reported that the differences in the respective impacts of 1.5 °C and 2 °C on various regional climate variables are significant, Karmalkar and Bradley (2017) claimed that the differences are marginal and negligible, especially when the associated uncertainties are compared with internal climate variability and inherent model diversity. However, there is a dearth of information on the potential impacts of these GWL on droughts in Southern Africa.

Although few studies have projected the impacts of the GWLs on regional droughts (e.g., James and Washington 2013; Maure et al. 2018), they only used precipitation as a proxy for such droughts. For instance, James and Washington (2013) analyzed CMIP5 General Circulation Models (GCMs) simulations and projected a decrease in precipitation over Southern Africa. They showed that the decreased precipitation is insignificant at 1 °C, but that the magnitude and spatial extents of the decrease become larger as the global warming increases to 2 °C and 4 °C. To improve on the GCM projections, Maure et al. (2018) analyzed the CORDEX regional climate model (RCM) projections (which have higher resolutions than the GCM projections) over Southern Africa and found that the decrease in precipitation has almost the same magnitude at 1.5 °C and 2.0 °C GWLs, although the decrease is more robust and covers a wider area at 2.0 °C. Nevertheless, these previous studies have two major limitations. Firstly, since they only used precipitation to characterize droughts, they do not account for the influence of PET on drought projections. The results may

thus underestimate the severity of future droughts over the subcontinent because PET (i.e., atmospheric demand for moisture) increases with atmospheric warming (Rind et al. 1990; Scheff and Frierson 2014). Secondly, the pattern of the precipitation projection provided in these studies is based on the multi-model simulation ensemble mean, which masked the different precipitation patterns. This makes it difficult to examine whether the projected precipitation pattern is a true representation of all the simulations, or whether it is dominated by few simulations with large precipitation changes. The present study builds on these previous studies by addressing the two shortcomings.

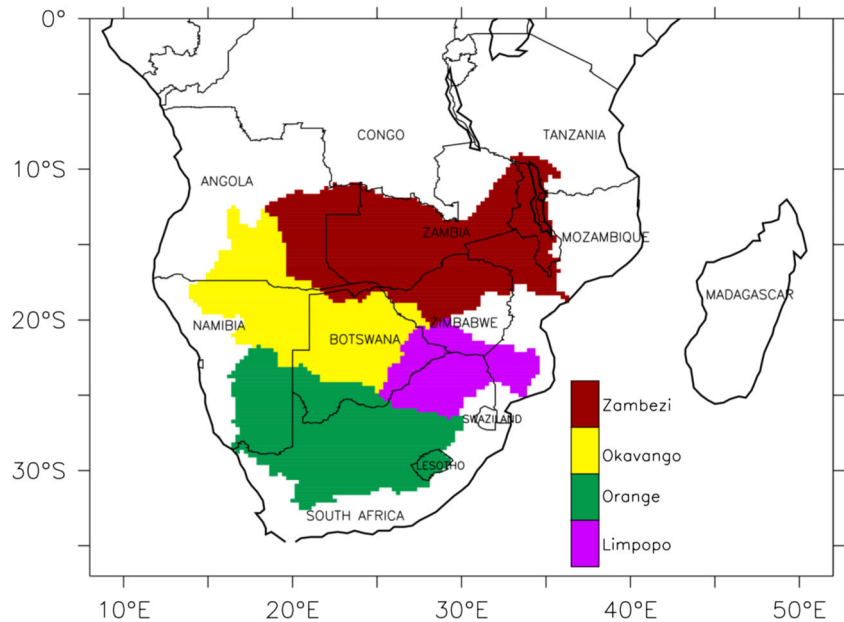
Hence, this study aims to investigate the potential impacts of GWLs on Southern African droughts, with an emphasis on droughts over four major river basins on the subcontinent. In the study, we analyze the multi-simulation datasets of the CORDEX RCMs to investigate the impacts at different GWLs (i.e., 1.5 °C, 2.0 °C, 2.5 °C, and 3.0 °C), use a drought index that is based on climate-water-balance to characterize the droughts, and employ self-organizing map (SOM) to group the projected droughts based on their similarities. Section 2 of the paper describes the data and methods used in the study, while Section 3 presents and discusses the results of the study, and Section 4 contains the concluding remarks.

2 Methodology

2.1 The study domain

Southern Africa, which is defined as the part of Africa that is bounded in the south by 40° S and in the north by the equator (Fig. 1), is characterized by high rainfall variability with recurrent floods and droughts. The highest temperatures (in excess of 40 °C) occur over the Kalahari Desert, which stretches over southeast Namibia, southwest Botswana and northwest South Africa. The daytime maximum temperatures can be extremely high (> 40 °C) and the night-time temperature much lower, making the diurnal temperature range very large (> 20 °C). Southern Africa has two distinct rain seasons, namely: a warm wet season in the summer (November–March) with the late summer (January to March) contributing 40% of the annual rainfall (Crétat et al. 2012), and a cold dry season during winter (April–October). However, the southwest region of South Africa has a Mediterranean climate with most rain falling during the dry winter season. The high climate variability in Southern Africa is due to the dominance of atmospheric low- and high-pressure systems; the seasonal migration of the inter-tropical convergence zone (ITCZ), which is known to influence the timing and intensity of rainfall, the complex regional topography and the influence of the warm Indian and cold Atlantic Oceans, which result in higher or lower rainfall (Davis and Vincent 2017). These circulation features give rise to various climate zones in Southern Africa, ranging from arid

Fig. 1 The study domain and the four major Southern African river basins (Orange, Limpopo, Zambezi, and Okavango river basins) used in the study



conditions in the west and a semi-arid climate over much of the central part of Southern Africa to subtropical humid conditions over the low-lying regions to the east and the north, and a Mediterranean climate in the southwestern portion of South Africa (Davis and Vincent 2017).

This study focuses on the catchment areas of four major river basins in Southern Africa (the Orange, Limpopo, Zambezi and Okavango river basins; Fig. 1). The river basins are important socio-economic drivers of the countries in their catchment area because all key economic activities, such as agriculture, mining, power generation, and industry are conducted within the basins. Moreover, river basins, such as the Zambezi and the Limpopo, attract tourists from around the world to come and witness the majestic Victoria Falls and the Big Five in the Kruger National Park. Furthermore, many climate change adaptation and mitigation projects, such as Resilience in the Limpopo Basin (RESLIM) and the Permanent Okavango River Basin Water Commission (OKACOM), have been implemented to develop these basins. The Orange River basin, the third largest river basin in Southern Africa, has a drainage area about 1,000,000 km² (www.dwaf.gov.za). It covers the entire area of Lesotho (3.4%), a large part of South Africa (64.2%) and the southern regions of Botswana (7.9%) and Namibia (24.5%) (www.orasecom.org). Mean daily temperatures range from about 12 °C in the highlands to more than 22 °C in the regions near the mouth with extreme temperatures of over 50 °C in the Namibian part of the basin being common (DWAF). The mean annual rainfall at source of the river (in the Lesotho Highlands) is more than 1800 mm, and the mean annual potential evaporation is 1100 mm. At the mouth of the river (in Alexander Bay), the mean annual rainfall is less than 50 mm while the mean annual potential evaporation is more than 3000 mm (DWAF).

The Limpopo River Basin (25° E'–35° E' and 19° S–27° S) has a catchments area of about 415,000 km². It is home to 14 million inhabitants in the four riparian countries: Zimbabwe (15%), Mozambique (20%), Botswana (20%), and South Africa (45%) (Earle et al. 2006; Trambauer et al. 2015). The basin has high spatial variation as annual rainfall ranges from 200–1200 mm year⁻¹ with 530 mm year⁻¹ on average across the region (Seibert et al. 2017). The Okavango river basin is an endorheic basin with a hydrologically active area of 390,000 km² covering Angola (51.7%), Namibia (33%), and Botswana (15.3%) (FAO 1997; Folwell et al. 2006). The average annual discharge of 10 km³ leaving the Angolan Highlands terminates in the Okavango delta (Folwell et al. 2006). The basin receives an annual rainfall range of about 355 mm year⁻¹ at the delta and 1320 mm year⁻¹ over the Angolan headwaters (FAO 1997). The Zambezi, which is the largest river basin in Southern Africa, covers about 1.37 million km² across eight countries: Zimbabwe, Zambia, Tanzania, Namibia, Mozambique, Malawi, Botswana, and Angola (Thiemig et al. 2012). The annual accumulated basin flow of the Zambezi is 108 × 10⁹ m³ of water outlet into the Indian Ocean (Spalding-Fecher et al. 2016). The annual rainfall ranges from about 700 mm year⁻¹ for the south-southwestern areas and up to 1200 mm/year. in the northern areas, with an average of 990 mm year⁻¹ (Thiemig et al. 2012).

2.2 Data

Both observation and simulation datasets were analyzed in the study. The observation dataset was obtained from the Climate Research Unit (CRU; version 4.01; Harris et al., 2014). The CRU dataset provides monthly climate data at a high-resolution (0.5 × 0.5) over the entire global landmass for the period 1901 to 2016.

The simulation datasets were obtained from CORDEX (Nikulin et al. 2018). They consist of 20 regional climate simulation datasets from six CORDEX RCMs. The RCMs downscaled eight GCM simulations for past and future climates (1950–2100) over Africa at $0.44^\circ \times 0.44^\circ$ horizontal grid size. Although there are simulation datasets for various emission scenarios (i.e., the RCP4.5, 8.5), we only analyzed the high emission scenario (i.e., RCP8.5) dataset, because it has the largest number of simulation ensemble members. And, given the current greenhouse gas emission trajectories, the RCP8.5 scenario seems to be the most realistic business-as-usual scenario. The GCMs and the downscaling RCMs for the 20 simulations are list in Table 1. Detailed information on the GCMs and RCMs, including their configuration and set up, are in Nikulin et al. (2012). From both datasets, the monthly precipitation and temperatures (i.e., maximum, minimum, and mean; Tmax, Tmin, and Tmean, respectively) over Southern Africa were analysed.

2.3 Methods

To evaluate the performance of the simulation datasets in reproducing the climate of Southern Africa, we compared the simulated climate data for the period 1971–2000 (hereafter, reference period) with the CRU observation data for the same period. However, the evaluation focused on the variables needed for calculating drought indices. To assess the impacts of climate change at various GWLs (i.e., 1.5 °C, 2.0 °C, 2.5 °C, and 3.0 °C), we calculated the difference between the climate data in the reference period (1971–2000) and the GWL periods (i.e., GWL minus

reference). Following Nikulin et al. (2018), a GWL period is defined as a 30-year period in which the climatology of the global mean temperature is higher than that of the pre-industrial baseline period (1861–1890) by the targeted global warming value (e.g., 1.5 °C, 2.0 °C, 2.5 °C, or 3.0 °C). As shown in Table 1, the 30-year GWL period varies with the GCMs simulations.

2.3.1 Characterizing droughts

Two drought indices were used to characterize droughts over Southern Africa. The first index is the Standardized Precipitation Evapotranspiration Index (SPEI; Vicente-Serrano et al. 2010a & b) while the second is the Standardized Precipitation Index (SPI; McKee et al. 1993a, b). Both indices have been frequently used for studying droughts worldwide (e.g., Guttman 1998, 1999; Abatan et al. 2017a, b, 2018) and over Southern Africa (Meque and Abiodun, 2015; Ujeneza and Abiodun 2015; Araujo and Abiodun, 2016). The indices are similar, except that SPI calculates the drought index based on precipitation (P) only, while SPEI does so by using climatic water balance, which is precipitation minus potential evapotranspiration (PET). PET is also known as atmospheric evaporative demand. As the inclusion of PET in the SPEI computation accounts for the global warming effect, SPEI is expected to yield better results than SPI in terms of drought identification (Vicente-Serrano et al. 2010a). Using monthly CRU observation and CORDEX data as input in the SPI and SPEI algorithms in R software (Begueria & Vicente-Serrano 2014), we obtained the observed and simulated drought indices at 12-month timescale (ending in March, which is the end of the rainfall

Table 1 The names of GCMs and the downscaling RCMs for the simulations used in the study

GCMs	Period of the global warming levels				Downscaling RCMs
	1.5 °C	2 °C	2.5 °C	3 °C	
CanESM2 ^(a)	1999–2028	2012–2041	2024–2053	2034–2063	RCA4 ⁽⁵⁾
CNRM-CM5 ^(b)	2015–2044	2029–2058	2041–2070	2052–2081	RCA4 ⁽⁵⁾ , CCLM ⁽²⁾ , ALADIN ⁽¹⁾
CSIRO-Mk3 ^(c)	2018–2047	2030–2059	2040–2069	2050–2079	RCA4 ⁽⁵⁾
EC-EARTH-r1 ^(d)	2003–2032	2021–2050	2035–2064	2046–2075	RACMO ⁽⁴⁾
EC-EARTH-r3 ^(e)	2006–2035	2023–2052	2036–2065	2047–2076	HIRHAM ⁽³⁾
EC-EARTH-r12 ^(f)	2005–2034	2021–2050	2034–2063	2047–2076	RCA4 ⁽⁵⁾ , CCLM ⁽²⁾
GFDL-ESM2M ^(g)	2020–2049	2037–2066	2052–2081	2066–2095	RCA4 ⁽⁵⁾
HadGEM2-ES ^(h)	2010–2039	2023–2052	2033–2062	2042–2071	RCA4 ⁽⁵⁾ , CCLM ⁽²⁾ , RACMO ⁽⁴⁾
IPSL-CM5AMR ⁽ⁱ⁾	2002–2031	2016–2045	2027–2056	2036–2065	RCA4 ⁽⁵⁾
MIROC5 ^(j)	2019–2048	2034–2063	2047–2076	2058–2087	RCA4 ⁽⁵⁾
MPI-ESM-LR ^(k)	2004–2033	2021–2050	2034–2063	2046–2075	RCA4 ⁽⁵⁾ , CCLM ⁽²⁾ , REMO ⁽⁶⁾
NorESM1-M ^(l)	2019–2048	2034–2063	2047–2076	2059–2088	RCA4 ⁽⁵⁾ , WRF ⁽⁷⁾

The corresponding 30-year period for various global warming levels (1.5 °C, 2 °C, 2.5 °C and 3.0 °C) are indicated. More detailed information on the GCMs, RCMs, and method for calculating the periods are in Déqué et al. (2017). The alphabets (a–l) and numbers (1–6) in brackets of the GCMs and RCMs (respectively) are used tags to represent the simulations (e.g., a5 represents CanESM2_RCA4 simulation)

season for most of part of Southern Africa). More details on how to calculate SPI and SPEI can be obtained from Beguería et al. (2014).

There are different methods for calculating PET, e.g., using the Penman–Monteith (PM; Monteith 1965), Hargreaves (HG; Hargreaves and Samani 1985), and Thornthwaite (TW; Thornthwaite 1948) methods. The Hargreaves method is preferred to the Thornthwaite method, because it overestimates PET with increasing air temperature (Donohue et al. 2010). The PM method is usually considered the best approach, but it requires extensive and long-term data (e.g., wind speed, solar radiation, relative humidity and temperature) that are not usually available. Hence, the HG method is recommended for calculating PET if the data required by PM method are not available. We thus used the HG method in this study, because the CORDEX simulation datasets do not have all the variables needed for the PM method. However, we compare the results of our observed PET and SPEI with those obtained using the PM method.

2.3.2 Assessing the robustness of climate change

We assessed the robustness of the projected climate change based on two conditions. Firstly, at least 80% of the simulation must agree on the sign of the change. Second, at least 80% of the simulations must indicate that the climate change is statistically significant (at 99% confidence level; using a *t* test, with respect to the climate variability of the reference period). We consider the climate change signal to be significant if both conditions are satisfied. These two methods have been previously used to indicate the robustness of the climate change signal (Klutse et al. 2018; Maure et al. 2018; Nikulin et al. 2018).

In addition, we employed the SOM to group the simulated climate change patterns into 12 nodes (i.e., major patterns) based on their similarities, and thus identifies the most common patterns among the simulations. The SOM belongs to a class of unsupervised neural network for clustering objects according to their similarity; therefore, it reduces the dimensionality of a given dataset (Skupin and Agarwal, 2008; Oettli et al. 2014). It is similar to the K-means clustering method (Everitt et al., 2011), but unlike the K-means, it creates an order between the units. For instance, a node (2) in the SOMs algorithm is close to nodes (1) and (3) and show a clear transition between them, but the same notion is not valid in the k-means clustering method, where the relationship between different clusters is not indicated (Skupin and Agarwal 2008; Wehrens, 2011). Using the climate change patterns (drought index and severe drought frequency) as the input data, the SOMs analysis was performed with the SOM_PAK 3.2 software (Kohonen et al. 1996). The SOM_PAK software was freely obtained from the Helsinki University of Technology (http://www.cis.hut.fi/research/som_pak/).

Here, we applied the SOMs analysis on two datasets separately, using 12 (4×3) nodes classification. The first dataset consists of all the projected changes in SPI and SPEI at the four GWLs (GWL1.5, GWL2.0, GWL2.5, and GWL3.0) for all the simulations. The second dataset is the same as the first but for projected changes in frequency of SPEI severe droughts (i.e., 12-month SPEI < -1.5) and of SPI severe droughts (i.e., 12-month SPEI < -1.5). For each analysis we obtained the contribution of each drought index (SPEI and SPI), each GWL, and each simulation in relation to each SOM node.

3 Results and discussion

3.1 Model evaluation

The CORDEX RCMs give a realistic simulation of all the necessary climate variables for quantifying droughts over Southern Africa (Figs. 2, 3, and 4). The models adequately simulate the spatial distribution of temperatures (Tmax, Tmin, and Tmean), precipitation (Pre), potential evapotranspiration (PET), and climate water balance (CWB) over the subcontinent (Figs. 2, 3, and 4). For all the variables, the correlation between the simulated and observed fields is high ($r \geq 0.75$) and significant (at 99% confidence level). The models capture the essential features in the observed fields. For example, they capture the temperature maxima (> 30 °C) over Democratic Republic of the Congo (DRC), the Botswana-Namibia-Angola-Zambia border, Mozambique, and Madagascar (Fig. 2a and 2b). They also reproduce the topographically induced temperature minimum (< 3 °C) along the escarpment of South Africa (Fig. 2d and 2e). In agreement with observation, they simulate precipitation maxima (> 136 mm year⁻¹) over the north-eastern part of the subcontinent and over East Madagascar, feature heavy precipitation (> 100 mm year⁻¹) along the ITCZ (Fig. 2j and 2k), and reproduce a PET maximum over the eastern half of the continent (Fig. 2m and 2n). In addition, they replicate the observed zonal gradient in precipitation and CWB south of 20° S. These climate features are induced by a complex mixture of local, global, tropical, and temperate atmospheric features (Reason et al., 2006). The ability of the simulations to reproduce the features suggests that the models capture the essential atmospheric mechanisms that control the Southern Africa climate.

Nevertheless, there are notable biases in the RCM ensemble mean (Fig. 2). The ensemble mean features a cold bias (up to 4 °C in Tmin and Tmax) over most parts of Southern Africa and a warm bias (about 4 °C) over the coast of Namibia and Angola (Fig. 2c and 2f). The cold bias translates to an underestimation of PET (about 40 mm year⁻¹) over most of the region, while the warm bias results in an overestimation of PET (about 40 mm year⁻¹) along the coast (Fig. 2f). The simulations also show a wet bias (about 40 mm year⁻¹) along the Angola coast and dry bias (about -50 mm year⁻¹) over DRC and South

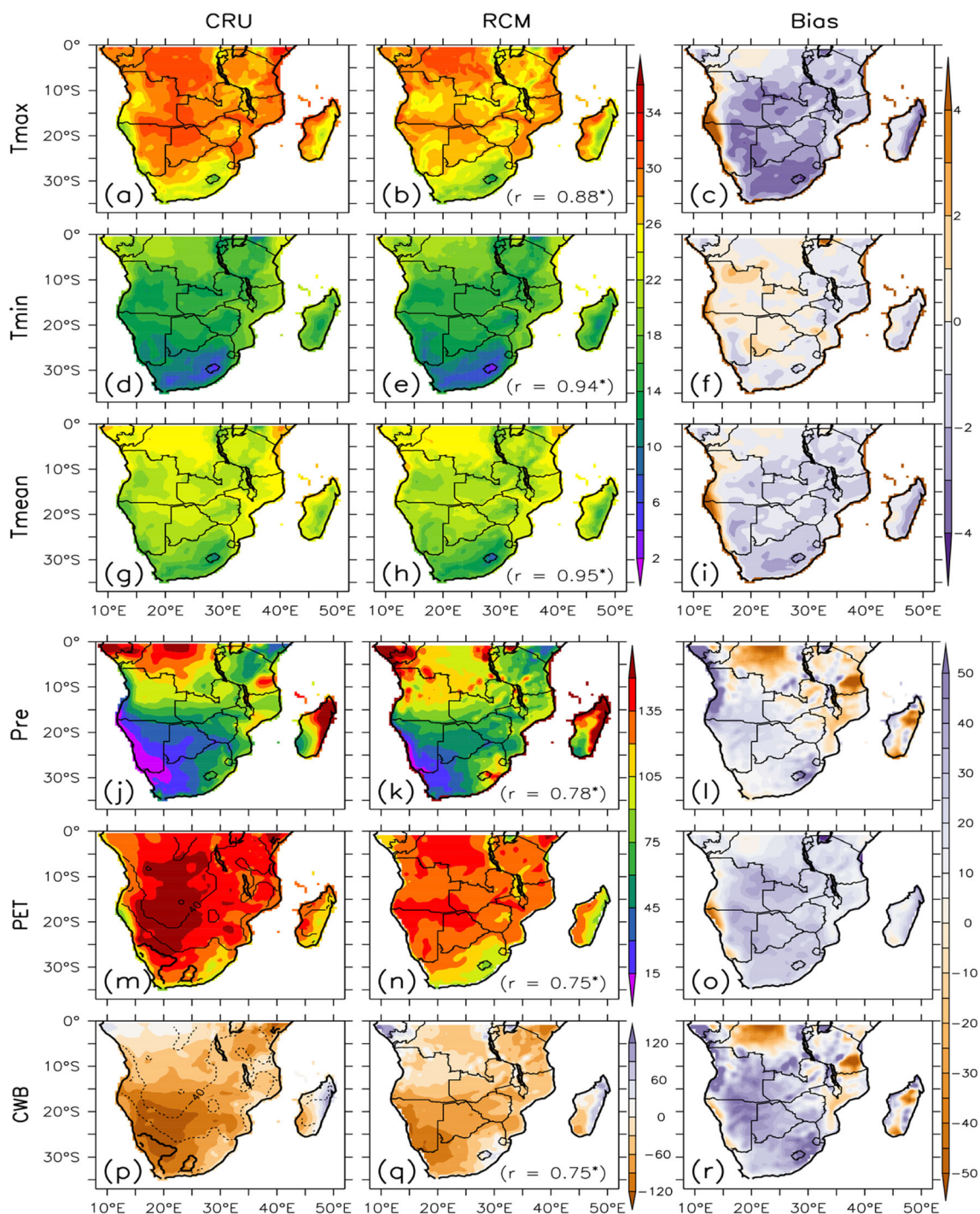


Fig. 2 The spatial distribution of climate variables over Southern Africa as depicted by CRU and CORDEX RCMs ensemble (RCM) in reference period (1971–2000). The climate variables are maximum temperature (T_{max} , °C), minimum temperature (T_{min} , °C), mean temperature (T_{mean} , °C), precipitation (Pre , mm month^{-1}), potential evapotranspiration (PET , mm month^{-1}), and climate water balance (CWB , mm

month^{-1}). The correlation (r) and difference (bias; $RCM-CRU$) between the observed and simulated variables are indicated. The asterisk (*) shows the correlation that is statistically significant at 99% confidence level. The contours on panels (m) and (p) indicate the difference between the results of Hargreaves and Penman methods (Hargreaves minus Penman; see the text for more information)

Tanzania (Fig. 2l). The errors in the precipitation and the PET fields produce a bias in the CWB distribution; this bias ranges from -50 mm year^{-1} over the DRC and along the east coast to 40 mm year^{-1} over most parts of Southern Africa (Fig. 2r).

However, while the negative bias in CWB is due to the underestimation of precipitation, the positive bias in CWB is caused by an underestimation of the PET . The discrepancy between the simulated and the observed fields can be attributed to many

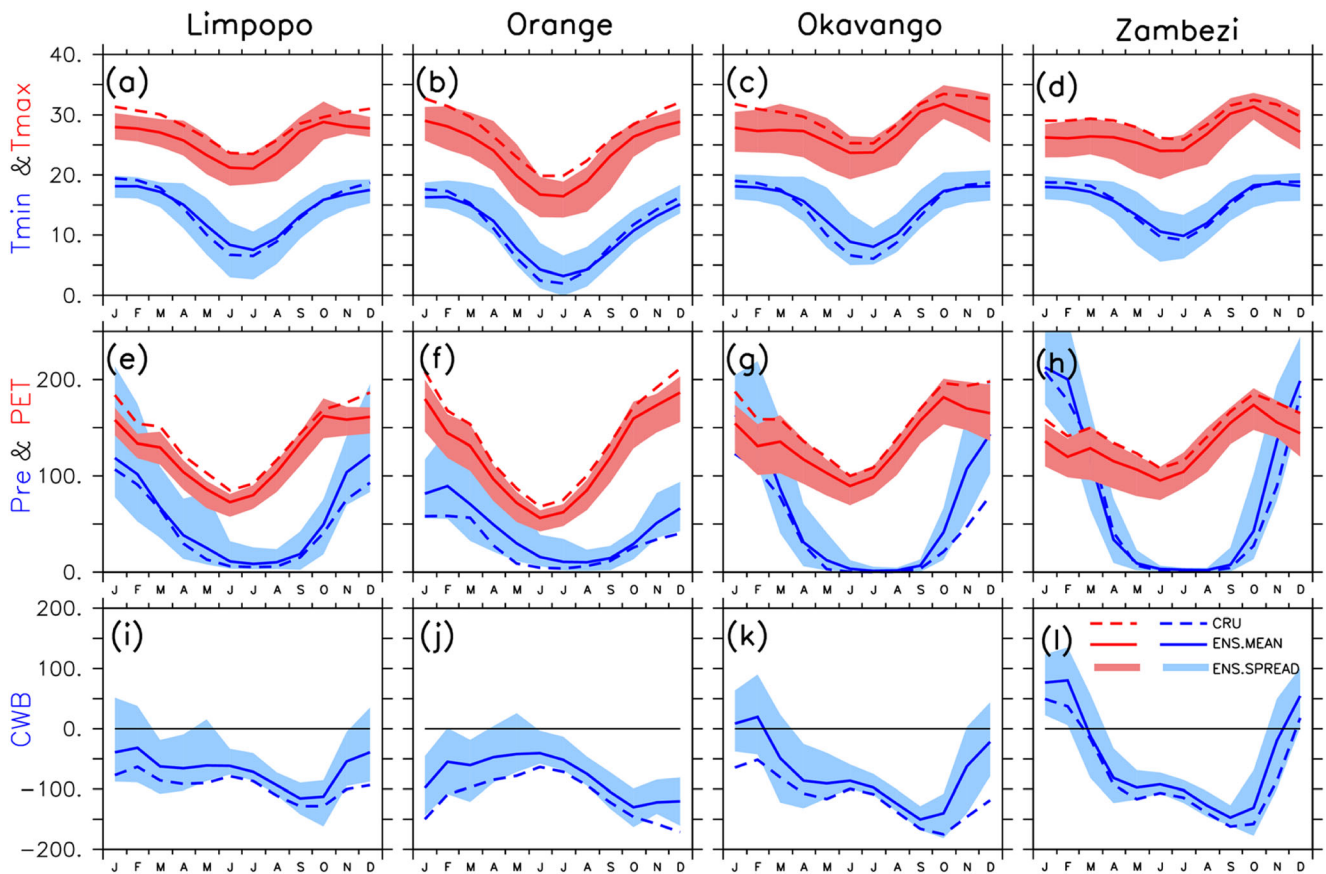


Fig. 3 The annual cycle of climate variables over the major river basins in Southern Africa (Limpopo, Orange, Okavango and Zambezi) depicted by CRU observation and CORDEX RCMs ensemble. The climate variables are maximum temperature (T_{max} , °C), minimum temperature (T_{min} ,

°C), mean temperature (T_{mean} , °C), precipitation (Pre, mm month^{-1}), potential evapotranspiration (PET, mm month^{-1}), and climate water balance (CWB, mm month^{-1})

factors. For example, the warm bias along the Angola coast suggests that the resolution of the models may be too low in capturing the influence of the Benguela Current and sea breeze on the temperature over the coast. The cold bias may be due to deficiencies in soil moisture parameterization in the models (Kalognomou et al. 2013). The wet bias over Angola and the dry bias over the DRC suggest that convective parameterization schemes in the models may be too active in producing precipitation over Angola, thereby making less moisture available for precipitation inland (i.e., over the DRC). Conversely, the discrepancy may be due to misrepresentation of observation data over Angola and the DRC where the density of weather station data is low (Munday and Washington 2017). The uncertainty in PET calculation may also contribute to the discrepancy. For example, note that the uncertainty in the observed PET (HG method minus PM method) is as high as the bias in the simulated PET (Fig. 2p).

Figure 3 shows that the RCMs also reproduce well the annual cycle of the climate variables over the river basins (i.e., Limpopo, Orange, Okavango, and Zambezi) as in CRU observation. In most cases, the observed annual cycle lies within the RCM ensemble spread and the ensemble mean curve closely follows the observed curve. Both the observed and the simulated cycles show

summer wet and winter dry conditions (Fig. 3e, f), reflecting the seasonal movement of the ITCZ over the sub-continent. All the basins experience their coldest and driest conditions (with PET) in from July to August, when the ITCZ is at its northern most position (i.e., in the northern hemisphere) and when the subsidence dominates over the basins. The monthly temperature and PET start to increase as from August when the ITCZ starts to retreat southward, but the rainy season over the basins only starts in October, when the ITCZ moves south of the equator and the subsidence over the subcontinent weakens (Reason, 2018). From October, the monthly precipitation increases rapidly and peaks in January–February (when the ITCZ reaches its southern most position); and from April, the monthly temperature and precipitation drop rapidly as the ITCZ moves back into the northern hemisphere. In both the observed and the simulated curves, the maximum deficit in CWB occurs in October over all the basins; the simulations agree with observation that the Limpopo and Orange river basins experience negative CWB (i.e., $PET > \text{precipitation}$) throughout the year, while the Okavango and Zambezi river basins experience negative bias in CWB from March to November. The most notable bias in the simulation occurs over the Limpopo river basin, where all the models

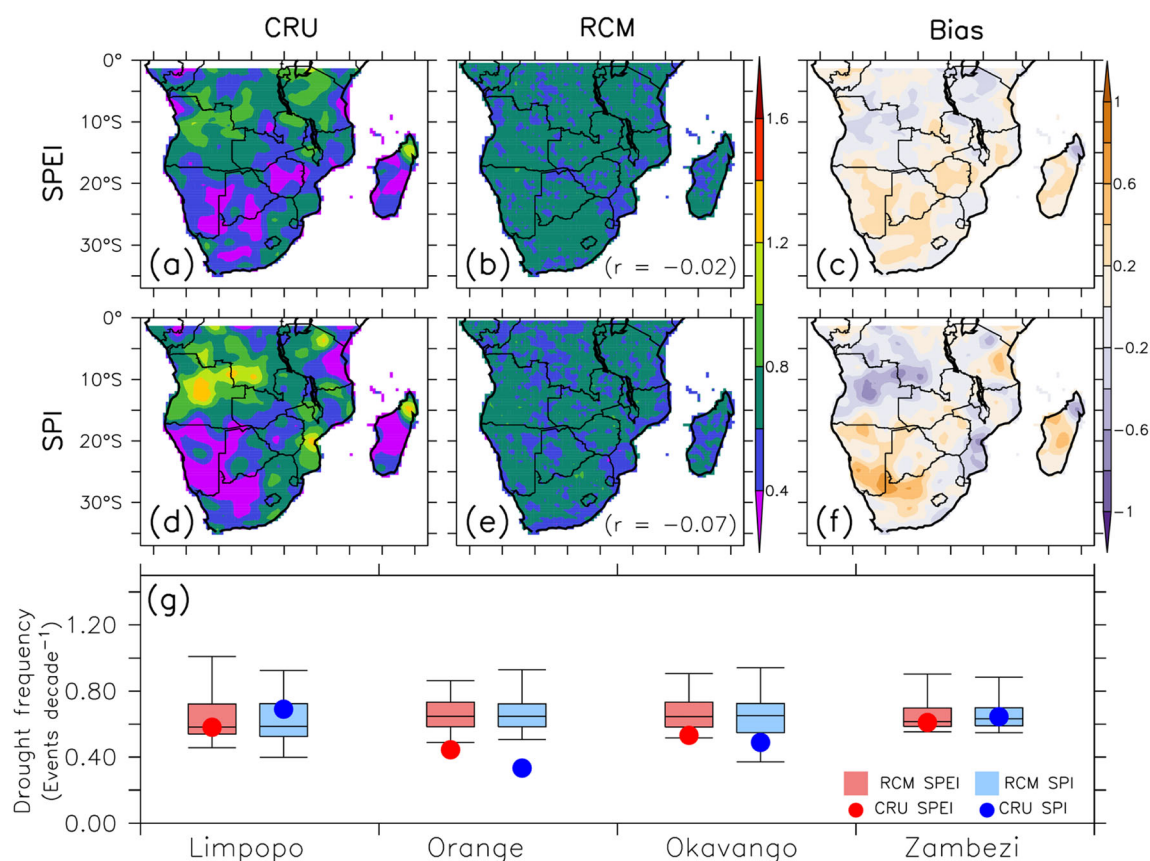


Fig. 4 The frequency of severe drought ($\text{SPEI} \leq -1.5$; $\text{SPI} \leq -1.5$) over Southern Africa (panels a–f) and over the major drought basins (Limpopo, Orange, Okavango, and Zambezi river basins; panel g), as depicted by CRU and CORDEX RCMs using SPEI and SPI to characterize droughts

overestimate the maximum temperature (in December–March, see Fig. 3a) and PET (in December–July, see Fig. 3e).

Despite the good performance of the RCM ensemble in simulating the spatial distribution of the climate variables (Fig. 2), the models struggle to reproduce the spatial variation of drought frequency over Southern Africa (Fig. 4). For both SPEI and SPI, the observation features a maximum drought frequency (> 0.8 events decade⁻¹) over Angola, the DRC, and Mozambique, and a minimum drought frequency (< 0.8 events decade⁻¹) over Namibia and South Africa. The RCM ensemble mean fails to reproduce this pattern ($r \approx 0.0$); instead, it shows a uniform severe drought frequency (0.4–0.6) over the region. Hence, the bias in the simulated drought frequency is up to 0.5 event decade⁻¹ (over South Africa and Namibia). This bias may be due to the averaging of the model results, because such averaging may filter out the spatial variability in each simulated pattern. This suggests a large discrepancy among the simulated patterns. Nevertheless, the models do capture well the magnitude of the drought frequency over the basin. The models perform best over the Limpopo and Zambezi river basins (where the observed frequency is within the inter-quartiles of the simulated frequency) and worst over the Orange river basin (where all the simulations overestimate the frequency).

3.2 Projected changes in drought characteristics under various global warming levels

At all warming levels, the CORDEX models project a decrease in SPEI (i.e., an increase in drought intensity) and an increase in SPEI drought frequency over Southern Africa (Fig. 5). However, with both drought intensity and frequency, the magnitude of the increase varies over the region and grows with increasing GWLs. At GWL1.5, the lowest increase in SPEI drought intensity ($\text{SPEI} \approx -0.3$) is projected over the tropical region while the highest increase ($\text{SPEI} < -0.9$) is shown over the southwestern coast (in Namibia and South Africa; see Fig. 5a), where the highest increase in the severe drought frequency (1 event decade⁻¹) is also projected (Fig. 5). At GWL2.0, the drought intensity over the southwestern coast increases by about 0.9, while the corresponding severe drought frequency increases by 2 events decade⁻¹. The increase in the drought intensity over the southwestern coast is robust (i.e., statistically significant at 99% confidence level) at GWL2.0 but not at GWL1.5. This suggests that keeping the global warming to 1.5 °C may limit the drought intensity within the natural variability of the reference climate. Conversely, a further increase in the warming level beyond

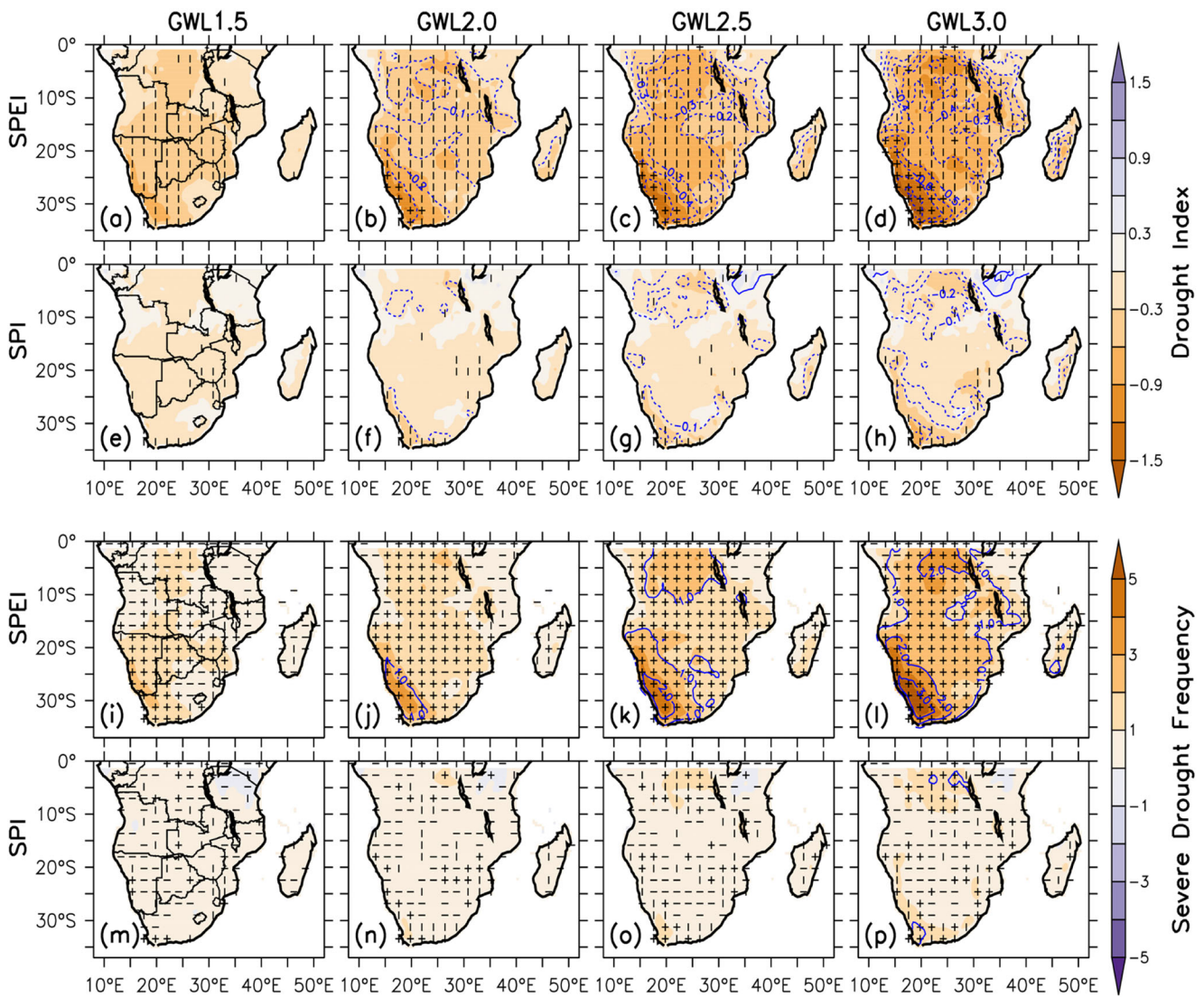


Fig. 5 Projected changes in drought index (for SPEI and SPI; panel a–h) and severe drought frequency (for SPEI and SPI; i–p) over Southern Africa at different global warming levels (GWL1.5, GWL2.0, GWL2.5, and GWL3.0). The vertical strip (|) indicates where at least 80% of the

simulations agree on the sign of the changes, while horizontal strip (–) indicates where at least 80% of the simulations agree that the projected change is statistically significant (at 99% confidence level). The cross (+) shows where both conditions are satisfied; hence, the change is robust

2.0 °C would enhance the drought intensity and frequency over the entire region, such that, at GWL3.0, more than half of South Africa and Namibia may be regarded a hotspot of severe droughts (Fig. 5). The maximum increase in SPEI-drought intensity and frequency over the southwest is consistent with the notion that global warming may reduce frontal precipitation over this area because of the poleward shift in mid-latitude cyclone tracks (Engelbrecht et al., 2009).

However, Fig. 5 shows that the projected changes in drought characteristics are sensitive to the drought indices (SPEI and SPI). For instance, in contrast to the SPEI, the SPI projects a decrease in drought intensity (i.e., more positive SPI) and frequency over the northeastern part of the region, and the magnitude of the decrease grows with increasing GWLs. Although both indices agree on the increase in

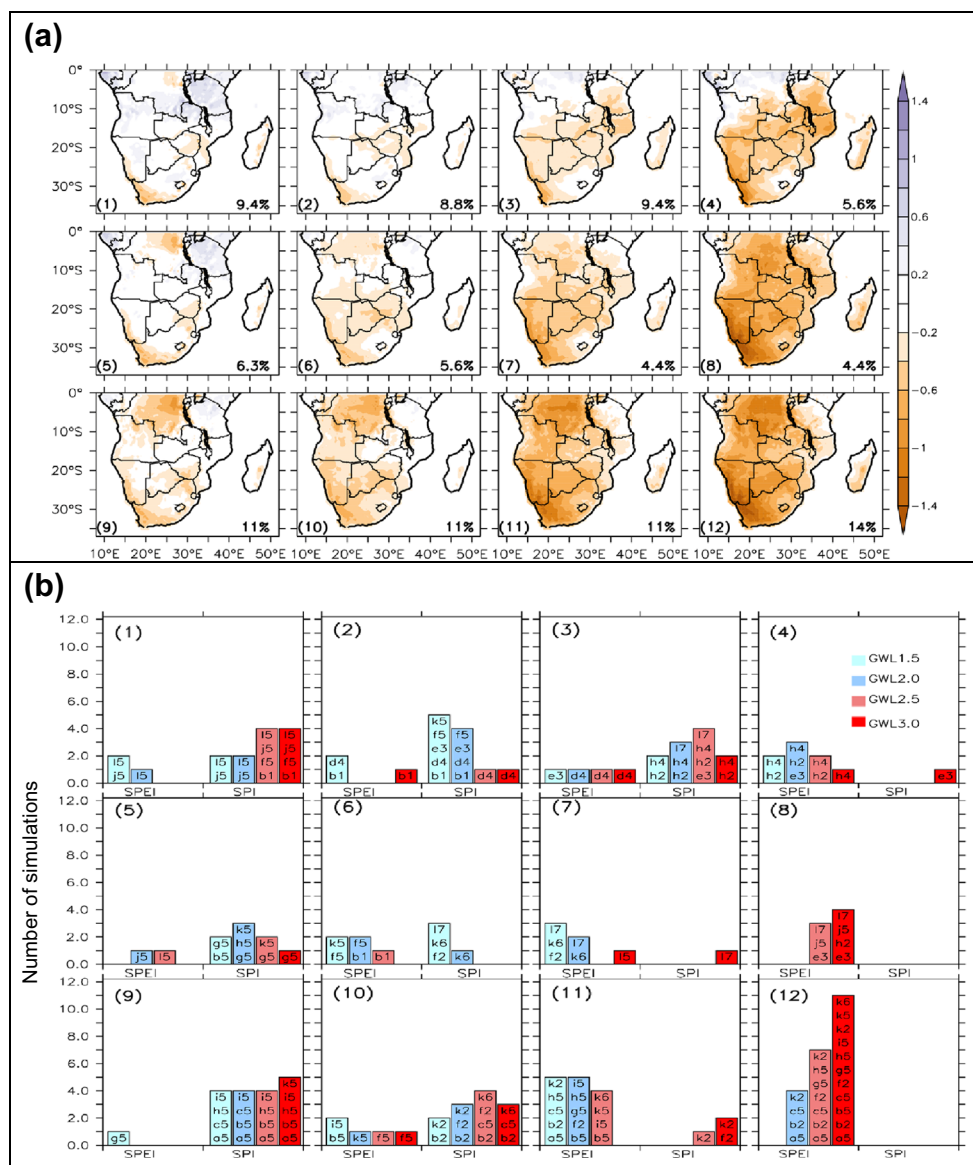
drought intensity and frequency over the remaining part of the subcontinent, the magnitude of the increase is smaller in the SPI projection, especially over the south-west coast. The discrepancy in drought intensity is up to 0.4 (at GWL1.5) and 1.2 (at GWL3.0), and that of drought frequency is up to 1.0 event decade⁻¹ (at GWL1.5) and 4 events decade⁻¹ (at GWL3.0). In addition, the increase in the drought intensity over the hotspot area is robust (i.e., statistically significant at 99% confidence level) for SPEI (from GWL2.0 upward), but not for SPI (at any GWL). Furthermore, the spatial variability of the projected changes is weaker in the SPI projections (where the drought intensity only ranges between 0.0 and –0.3 at GWL1.5; Fig. 5a) than in the SPEI projection (where the drought intensity ranges between –0.3 and –0.9 at GWL1.5, see Fig. 5e).

The weak changes in projected SPI droughts in this study agree with the weak changes in annual precipitation reported in the past studies (e.g., Engelbrecht et al., 2009; Haensler et al., 2013, Maure et al., 2018). For instance, Engelbrecht et al. (2009) project less than < 10% changes in annual precipitation over Southern Africa in the future (2070–2100) under the A2 scenario, while Maure et al. (2018) also found the same at both GWL1.5 and GWL2.0 levels. However, the present study shows that accounting for atmospheric evaporative demand (PET) in the drought projections (i.e., using SPEI) produces more severe droughts than using only precipitation (or SPI) for the projection. Arguably, the SPEI projection might have overestimated the magnitude of the changes, because the water balance calculation is based on PET rather than actual evapotranspiration (ET). However, the goal of SPEI is to obtain the maximum drought stress over a surface

by comparing the highest ET (i.e., atmospheric water demand) with water available (i.e., precipitation) over the surface (Beueria et al., 2014). Hence, using ET is not a good estimator of atmospheric water demand because ET also depends on water availability and on the characteristics of the surface. In addition, by definition (Allen et al., 1998), both PET and ET are the same over a well-watered surface (e.g., hypothetical grass reference crop and open water). However, it is essential to use both SPI and SPEI for drought projection, because while the SPI projection provides information about the lower limits of the drought stress, the SPEI will provide information on the upper limits of drought stress.

The SOM classification indicates that the spatial patterns of changes in the drought index (Fig. 6) and in the drought frequency (Fig. 7) vary among the simulations. As is typical of SOM classification, the most extreme patterns are indicated at

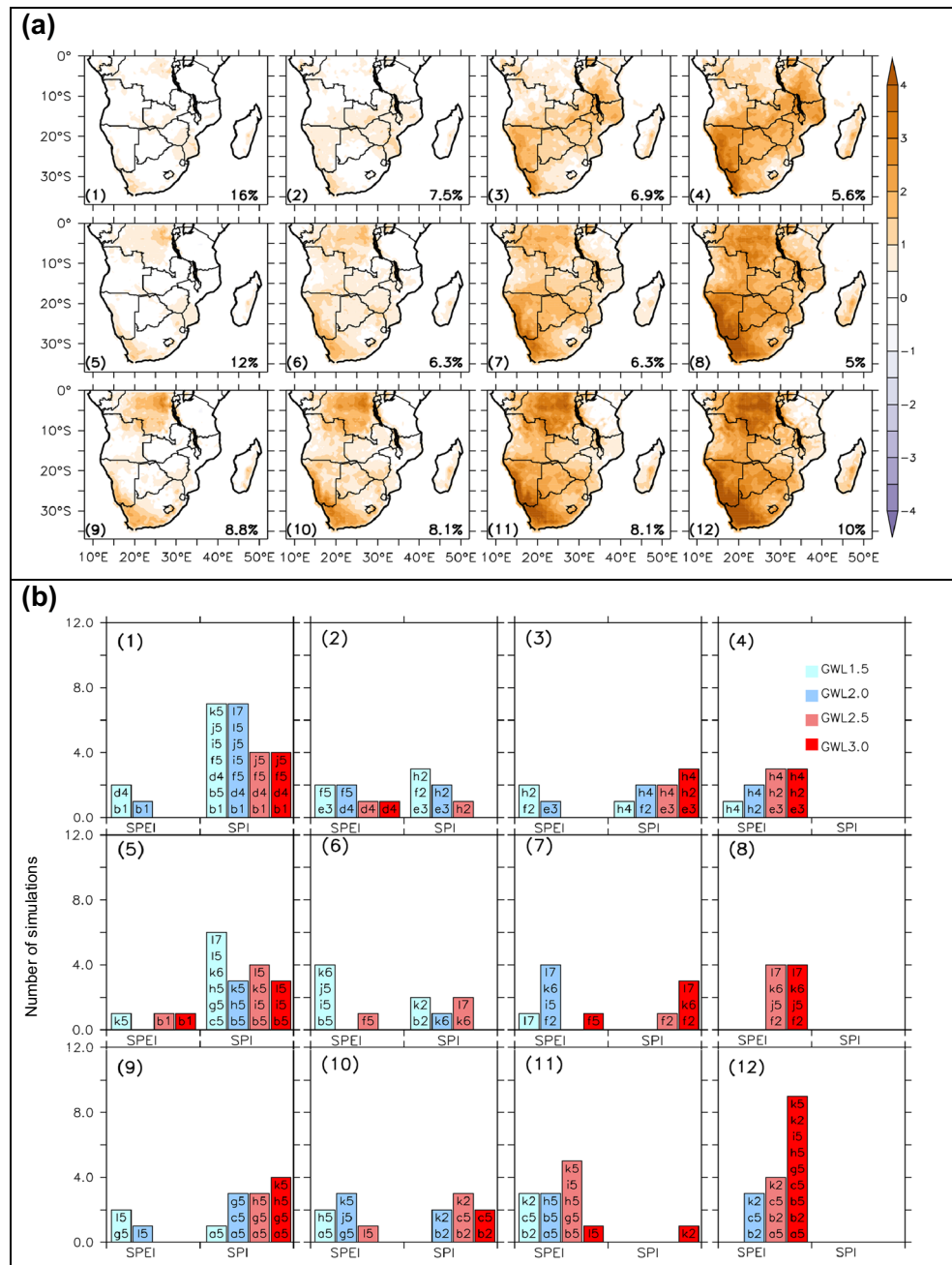
Fig. 6 a The SOMs distribution (3 × 4 nodes) of pattern of projected changes in drought index (SPEI; SPI) over Southern Africa at different GWLs (GWL1.5, GWL2.0, GWL2.5, and GWL3.0), as depicted by CORDEX simulation dataset. The numbers at the lower-left and lower-right corners show tag and percentage contribution of each pattern in the dataset, respectively; **b** the frequency of the patterns under each GWL, drought index, and simulation. The codes in each bar are the tags of the simulations make up the bar. In a simulation tag, alphabet indicates the GCM while the number denotes the RCM (e.g., a5 represents CanESM2_RCA4 simulation), see Table 1



the edge nodes (1, 4, 9, and 12), while patterns in other nodes are smooth transition among the extreme patterns. Node 12, which features the largest magnitude of changes in drought indices, shows a decrease in the drought index over most of Southern Africa, with the largest decrease (about -1.4) in the southwestern and tropical-western parts of the subcontinent. With SPEI, the number of simulations that project this pattern increases with increasing GWLs; while no simulation projects it at GWL1.5, 11 simulations do indicate it at GWL3.0. In contrast, no simulation indicates this for SPI at any GWL. Node 4 has a similar pattern as Node 12, but it features the largest increase in the southwestern and tropical-eastern parts

of the subcontinent. With SPEI, two simulations project Node 4 at GWL1.5 and GWL2.5, three at GWL2.5, but one at GWL3.0. Only one simulation indicates it for SPI (i.e., at GWL3.0). In contrast to Nodes 4 and 12, Nodes 1 and 2 are characterized by weak changes (i.e., within ± 1) in the drought index. Although both nodes (i.e., 1 and 9) indicate their maximum drying condition (negative drought index) over the southwestern areas, they feature different results in the tropics, where Node 1 features pluvial (positive drought index) while Node 9 shows drying conditions. However, these nodes are more projected for SPI than for SPEI. Similar results are obtained in the drought frequency classification (Fig. 7).

Fig. 7 Same as Fig. 6, except for drought frequency



For both drought intensity and frequency (Figs. 6 and 7), the distinction between the change in SPEI and SPI drought patterns is clear in the simulations, except in a few cases. The few simulations that mix the patterns do so at GWL1.5 and GWL2.0 (Fig. 6). For example, in terms of drought intensity (Fig. 6), at GWL1.5 and GWL2.0, two simulations (i.e., i5 and j5: IPSL_RCA and MIROC5_RCA4, respectively) feature both SPEI and SPI patterns to Node 1, and another two (i.e., d4 and b1: EC-Earth-r1_RACMO and CNRM-CM5_ALADIN) allocate them to Node 2. Also, in the drought frequency patterns (Fig. 7) at GWL1.5 and GWL2.0, two models (b1 and d4: CNRM_ALADIN and EC-EARTH-r1_RACMO) show both SPEI and SPI patterns in Node 1. Nevertheless, the separation between the SPEI and SPI drought patterns is well established by all the simulations at GWL2.5 and GWL3.0. This implies that the magnitude of evaporation-induced droughts increases with increasing GWLs.

The level of agreement among the simulations (which is a measure of robustness, see Pfeifer et al. 2015) on the drought projections over the river basins also depends on the drought indices (SPEI and SPI). In general, agreement among the simulations is better for SPEI projections than for SPI projection. For instance, over Limpopo, all the simulations agree on the SPEI projections at GWL2.5 and GWL3.0 (Fig. 8a), but they do not agree on the SPI projections. The same is true over the Orange and Okavango river basins. The least agreement among the simulations occurs over the Zambezi basin, where more than 75% of the simulations agree on the SPEI projection but less than 75% agree on SPI projection. The large uncertainty in the SPI

drought projection reported here agrees with previous studies on precipitation (e.g., Maure et al., 2018). This indicates that combining PET with precipitation in determining future droughts over Southern Africa improves the robustness of the drought projection. This is due to the inherent robust signal in the temperature projection over the subcontinent (Maure et al. 2018).

Nevertheless, the differences between the SPEI and SPI projections have implications for combating future drought risks over the basins in two ways. Firstly, the better robustness of the SPEI projection lowers the level of uncertainty in future drought projection and provides more reliable evidence for embarking on adaptation strategies toward reducing future drought risks. Secondly, with SPI projection information, little or nothing can be done at basin level to mitigate drought impacts, because the amount of precipitation received in a basin does not significantly depends on the management of the basin, especially in the case of a small river basin. Conversely, a comparison of SPEI and SPI projection indicates that evaporation can make a future drought more severe than indicated by the SPI projections. Therefore, any basin management practices that can minimize future ET over a river basin would help to lower the future drought risk in that basin. For example, well-planned land-cover changes can be used to reduce the additive effects of ET on drought over river basins, although this depends on the type and degree of landuse (Lumsden et al. 2003). Many studies have documented how landuse change can be used to influence the hydrological cycles over a basin (e.g., Gyamfi et al. 2016; Zhang et al. 2008; Pervez and Henebry 2015; Yin et al. 2017). For instance, the healthy riparian zone can provide shading and minimize evaporation from the water resources (Bellows 2003).

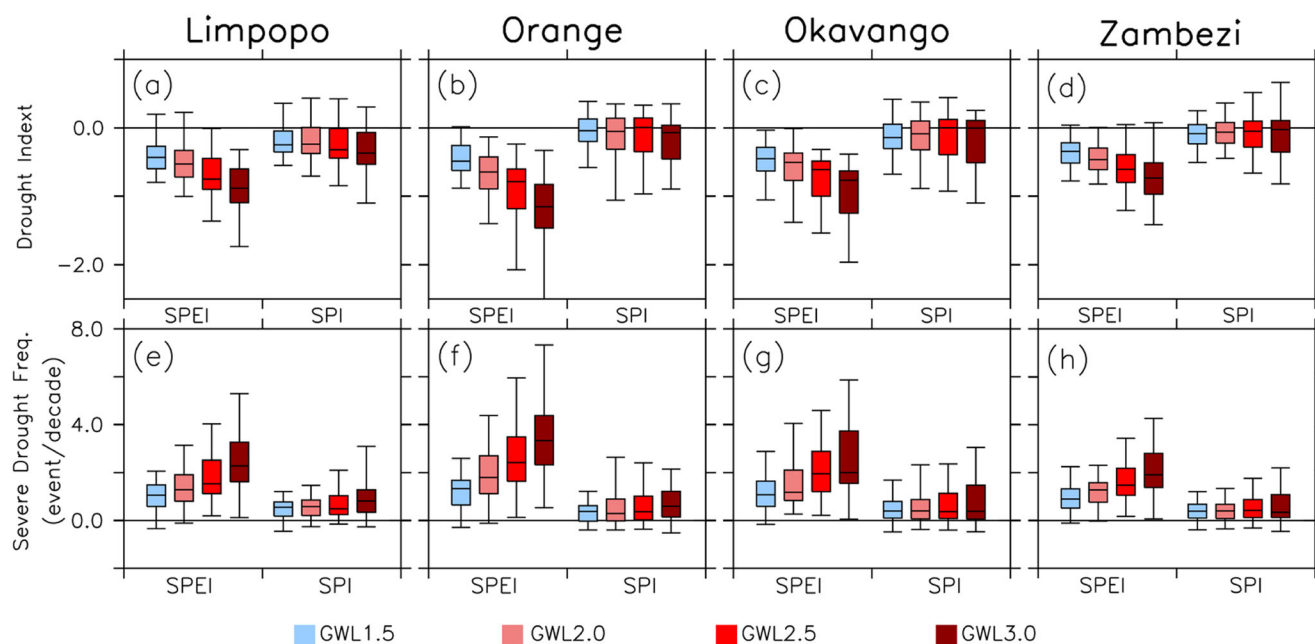


Fig. 8 Projected changes in drought index (panels a–d; for SPEI and SPI) and severe drought frequency (panels e–h; for SPEI and SPI) over the four major river basins in Southern Africa (Limpopo, Orange, Okavango, and Zambezi)

3.3 Implications for strategy policy

The above result provides a basis for developing policy and strategy to reduce future drought risks over Southern African river basins. At the same time, it advocates for a more proactive response to increase resilience and adaptive options. For instance, the analysis of both SPI and SPEI indicates that a greater proportion of the Southern Africa region may become drier in the future, mainly because increased PET would enhance evaporation losses from dams and increase irrigation demands for drier soils. This will have negative impacts on regional development, as economic activities (e.g., agriculture, industrial water supply, tourism) will take longer than usual to recover after each drought episode. The increasing population also implies that demand for water may escalate. However, the analysis also suggests that a well-planned land-use change (that is targeted to limit evaporation losses) could help to reduce the impacts of the projected droughts. Hence, there is a need for the formulation of strategic policy that can accommodate or encourage such a land-use change. Strategic policy is also required on other drought-related issues like drought-induced migration (environmental refugees), drought impacts on economic hubs, infrastructure challenges, population growth, and more importantly the new opportunities that may arise out of the droughts. Hence, the results can guide policymakers on how to prioritize and redefine future economic possibilities.

4 Conclusion

We have analyzed multi-simulation datasets from CORDEX RCMs to quantify the impacts of global warming on future droughts over Southern Africa, focusing on the four major river basins and on four global warming levels (i.e., 1.5 °C, 2.0 °C, 2.5 °C, 3.0 °C) above the pre-industrial level. We used two drought indices (SPEI and SPI) to characterize the droughts and used SOMs to group the projected changes in drought index and severe drought frequency into 12 groups, based on their similarities. Before examining the RCM-projected changes in future droughts, we evaluated the capability of the models in simulating the Southern Africa climate during the reference period (1971–2000). Our results can be summarized as follows:

- The CORDEX ensemble provides a good representation of the Southern African climate, though with some biases. While the RCMs capture all the essential features in the spatial distribution of the climate variables over the sub-continent, they struggle to reproduce the spatial variation of the severe drought frequency as in observation.

- The models replicate the observed annual cycle of the climate variables over the four basins, although they all overestimate Tmax and PET over the Limpopo river basin.
- An increase in SPEI (i.e. drought intensity) is projected over Southern Africa under the four GWLs. The increase is insignificant at GWL1.5, but significant over the southwestern part of the subcontinent at GWL2.0. The magnitude and significant areas of the increase grow with further warming. In contrast, change in SPI is not significant at any GWLs, and the magnitude of the increase is lower than that of SPEI.
- For both SPEI and SPI, the projected changes in drought frequency are significant, but the magnitude of the changes in SPI drought frequency is lower than that of SPEI drought frequency.
- The SOM classification reveals that most simulations clearly distinguished between the projected changes in SPEI and SPI drought patterns over Southern Africa. However, the distinction becomes clearer with increasing GWLs.
- The projected changes in drought characteristics over the river basins are more robust with SPEI than with SPI. A combination of both projections is thus needed in quantifying and mitigating the impacts of evapotranspiration-induced droughts in the warmer future climate.

The results of this study can be improved and applied to reduce future drought risks over Southern Africa in many ways. For instance, the uncertainty (i.e., the disagreement among the models) in the drought projections may be further reduced by reducing the biases in both GCMs and RCMs simulations. More focused studies on how to reduce the uncertainty will improve the credibility and application of the results. Future studies could examine the contribution of atmospheric processes to the differences in SPEI and SPI projections; the lack of relevant upper-level dynamic data in the CORDEX archive hindered such analysis in the present study. In addition, there is a need to extend this meteorological drought projection to hydrological droughts (i.e., stream flows) in the river basins. Such studies will make the results more relevant for policy makers. However, the present study has shown that using only SPI to characterize future droughts may underestimate the drought severity and frequency but using both SPEI and SPI would help in quantifying evaporative-induced droughts and in mitigating the impact of climate change on droughts in the future.

Acknowledgements The study was supported with research grants from the Water Research Commission (WRC, South Africa) and National Research Foundation (NRF, South Africa). The Centre for High Performance Computing (CHPC, South Africa) provided the computing facility used for the study.

Publisher's Note Springer Nature remains neutral with regard to jurisdictional claims in published maps and institutional affiliations.

References

- Abatan AA, Gutowski WJ Jr, Ammann CM, Kaatz L, Brown BG, Buja L, Bullock R, Fowler T, Gilleland E, Gotway JH (2017a) Multi-year droughts and pluvials over Upper Colorado River basin and associated circulations. *J Hydrometeorol* 18:799–818. <https://doi.org/10.1175/JHM-D-16-0125.1>
- Abatan AA, Gutowski WJ Jr, Ammann CM, Kaatz L, Brown BG, Buja L, Bullock R, Fowler T, Gilleland E, Halley Gotway J (2017b) Statistics of multi-year droughts from the method for object-based diagnostic evaluation (MODE). *Int J Climatol* 38(8):3405–3420. <https://doi.org/10.1002/joc.5512>
- Abatan AA, Abiodun BJ, Gutowski WJ, Rasaq-Balogun SO (2018) Trends and variability in absolute indices of temperature extremes over Nigeria: linkage with NAO. *Int J Climatol* 38(2):593–612
- Allen RG, Pereira LS, Raes D, Smith M (1998) Crop evapotranspiration—Guidelines for computing crop water requirements—FAO Irrigation and drainage paper 56. Fao, Rome 300(9):D05109
- Araujo JA, Abiodun BJ, Crespo O (2016) Impacts of drought on grape yields in Western Cape, South Africa. *Theor Appl Climatol* 123(1–2):117–130
- Beguéría S, Vicente-Serrano SM, Reig F, Latorre B (2014) Standardized precipitation evapotranspiration index (SPEI) revisited: parameter fitting, evapotranspiration models, tools, datasets and drought monitoring. *Int J Climatol* 34(10):3001–3023
- Bellows BC (2003) Protecting riparian areas: farmland management strategies. Appropriate technology transfer for rural areas. Davis, CA
- Blench R, Marriage Z (1999) Drought and livestock in semi-arid Africa and southwest Asia. Working Paper 117. Overseas Development Institute, London, p 138
- Botai CM, Botai JO, de Wit JP, Ncongwane KP, Adeola AM (2017) Drought characteristics over the Western Cape Province, South Africa. *Water* 9(11):876
- Calow RC, MacDonald AM, Nicol AL, Robins NS (2010) Ground water security and drought in Africa: linking availability, access, and demand. *Groundwater* 48(2):246–256
- Crétat J, Pohl B, Richard Y, Drobinski P (2012) Uncertainties in simulating regional climate of Southern Africa: sensitivity to physical parameterizations using WRF. *Clim Dyn* 38(3–4):613–634
- Dai A (2011) Drought under global warming: a review. *Wiley Interdiscip Rev Clim Chang* 2(1):45–65
- Davis CL, Vincent K (2017) Climate risk and vulnerability: a handbook for Southern Africa, 2nd edn. CSIR, Pretoria
- Donohue RJ, McVicar TR, Roderick ML (2010) Assessing the ability of potential evaporation formulations to capture the dynamics in evaporative demand within a changing climate. *J Hydrol* 386(1–4):186–197
- Donnelly C, Greuell W, Andersson J, Gerten D, Pisacane G, Roudier P, Ludwig F (2017) Impacts of climate change on European hydrology at 1.5, 2 and 3 degrees mean global warming above preindustrial level. *Clim Chang* 143(1–2):13–26
- DWAF, Department of Water Affairs and Forestry, South Africa (Website) Introduction to the Orange River Basin. Online available at: www.dwaf.gov.za/orange/. Accessed 11 Nov 2018
- Earle A, Goldin J, Machiridza R et al (2006) Indigenous and institutional profile: Limpopo river basin, vol. 112. International Water Management Institute, Colombo
- Engelbrecht FA, McGregor JL, Engelbrecht CJ (2009) Dynamics of the Conformal-Cubic Atmospheric Model projected climate-change signal over southern Africa. *Int J Climatol* 29(7):1013–1033
- Everitt, B.S., Landau, S., Leese, M. and Stahl, D., (2011). Cluster analysis: Wiley series in probability and statistics.
- FAO (1997) FAO land and water bulletin. In: Frenken K and Faurès JM(1997) Irrigation potential in Africa: A Basin Approach. FAO Land and Water Bulletin, Vol. 4, Food & Agriculture Organization
- Folwell S, Farquharson F, Demuth S, Gustard A, Planos E, Seatena F, Servat E (2006) The impacts of climate change on water resources in the Okavango basin. IAHS Publ 308:382
- Gosling SN, Zaherpour J, Mount NJ, Hattermann FF, Dankers R, Arheimer B, Breuer L, Ding J, Haddeland I, Kumar R, Kundu D (2017) A comparison of changes in river runoff from multiple global and catchment-scale hydrological models under global warming scenarios of 1 C, 2 C and 3 C. *Clim Chang* 141(3):577–595
- Guttman NB (1998) Comparing the Palmer drought index and the Standardized Precipitation Index. *J Am Water Resour Assoc* 34:113–121
- Guttman NB (1999) Accepting the Standardized Precipitation Index: a calculation algorithm. *J Amer Water Resources Assoc* 35:311–322
- Gyamfi C, Ndambuki JM, Salim RW (2016) Hydrological responses to land use/cover changes in the Olifants Basin, South Africa. *Water* 8(12):588
- Haensler A, Saeed F, Jacob D (2013) Assessing the robustness of projected precipitation changes over central Africa on the basis of a multitude of global and regional climate projections. *Clim Chang* 121(2):349–363
- Hargreaves GL, Samani ZA (1985) Reference crop evapotranspiration from temperature. *Appl Eng Agric* 1:96–99
- Harris IPDJ, Jones PD, Osborn TJ, Lister DH (2014) Updated high-resolution grids of monthly climatic observations—the CRU TS3. 10 Dataset. *Int J Climatol* 34(3):623–642
- Hulme M (2016) 1.5 C and climate research after the Paris agreement. *Nat Clim Chang* 6(3):222–224
- IPCC (2007) The physical science basis. In: Solomon S, Qin D, Manning M, Chen Z, Marquis M, Averyt KB, Tignor M, Miler HL (eds) Contribution of working group I to the fourth assessment report of the International Panel on Climate Change Program. Cambridge University Press, Cambridge, p 996
- James R, Washington R (2013) Changes in African temperature and precipitation associated with degrees of global warming. *Clim Chang* 117(4):859–872
- Kalognomou EA, Lennard C, Shongwe M, Pinto I, Favre A, Kent M, Hewitson B, Dosio A, Nikulin G, Panitz HJ, Büchner M (2013) A diagnostic evaluation of precipitation in CORDEX models over Southern Africa. *J Clim* 26(23):9477–9506
- Karmalkar AV, Bradley RS (2017) Consequences of global warming of 1.5 C and 2 C for regional temperature and precipitation changes in the contiguous United States. *PLoS One* 12(1):e0168697
- Klutse NAB, Ajayi VO, Gbobaniyi EO, Egbebiyi TS, Kouadio K, Nkrumah F, Quagrainne KA, Olusegun C, Diasso U, Abiodun BJ, Lawal K (2018) Potential impact of 1.5° C and 2° C global warming on consecutive dry and wet days over West Africa. *Environ Res Lett* 13(5):055013
- Kohonen T, Hynninen J, Kangas J, Laaksonen J (1996) Som pak: The self-organizing map program package. Report A31, Helsinki University of Technology, Laboratory of Computer and Information Science.
- Kusangaya S, Warburton ML, Archer Van Garderen E, Jewitt GPW (2014) Impacts of climate change on water resources in southern Africa: A review. *Phys Chem Earth Parts A/B/C* 67–69:47–54
- Lumsden TG, Jewitt GPW, Schulze RE. (2003) Modelling the Impacts of Land Cover and Land Management Practices on Runoff Responses. Water Research Commission, RSA, Report 1015/1/03
- Maure G, Pinto I, Ndebele-Murisa M, Muthige M, Lennard C, Nikulin G, Dosio A, Meque A (2018) The Southern African climate under 1.5° C and 2° C of global warming as simulated by CORDEX regional climate models. *Environ Res Lett* 13(6):065002
- Masih I, Maskey S, Mussá FEF, Trambauer P (2014) A review of droughts on the African continent: a geospatial and long-term perspective. *Hydrol Earth Syst Sci* 18(9):3635–3649
- McKee TB, Doesken NJ, Kleist J (1993a) The relationship of drought frequency and duration to time scales. Preprints, Eighth Conf. on Applied Climatology, Anaheim, CA, Amer Meteor Soc, 179–184

- McKee TB, Doesken NJ, Kleist J (1993b) The relationship of drought frequency and duration to time scales. In Proceedings of the 8th Conference on Applied Climatology, vol. 17, No. 22, American Meteorological Society, Boston, pp 179–183
- Meque A, Abiodun BJ (2015) Simulating the link between ENSO and summer drought in Southern Africa using regional climate models. *Clim Dyn* 44(7-8):1881–1900
- Mishra AK, Singh VP (2010) A review of drought concepts. *J Hydrol* 391(1–2):202–216
- Mniki S (2009) Socio-economic impact of drought induced disasters on farm owners of Nkonkobe local municipality (Doctoral dissertation, University of the Free State).
- Monteith JL (1965) Evaporation and environment. The state and movement of water in living organisms. In: Fogg GE (ed) *Sympos. Soc. Exper. Biol.* 19, Academic Press, N.Y. 1965, pp. 205–234
- Munday C, Washington R (2017) Circulation controls on Southern African precipitation in coupled models: the role of the Angola Low. *J Geophys Res-Atmos* 122(2):861–877
- Nikulin G, Jones C, Giorgi F, Asrar G, Büchner M, Cerezo-Mota R, Christensen OB, Déqué M, Fernandez J, Hänsler A, van Meijgaard E (2012) Precipitation climatology in an ensemble of CORDEX-Africa regional climate simulations. *J Clim* 25(18):6057–6078
- Nikulin G, Lennard C, Dosio A, Kjellström E, Chen Y, Hänsler A, Kupiainen M, Laprise R, Mariotti L, Maule CF, van Meijgaard E (2018) The effects of 1.5 and 2 degrees of global warming on Africa in the CORDEX ensemble. *Environ Res Lett* 13(6):065003
- Oettli P, Tozuka T, Izumo T, Engelbrecht FA, Yamagata T (2014) The self-organizing map, a new approach to apprehend the Madden-Julian Oscillation influence on the intraseasonal variability of rainfall in the southern African region. *Clim Dyn* 43(5-6):1557–1573
- Pfeifer S, Bülow K, Gobiet A, Hänsler A, Mudelsee M, Otto J, Rechid D, Teichmann C, Jacob D (2015) Robustness of ensemble climate projections analyzed with climate signal maps: seasonal and extreme precipitation for Germany. *Atmosphere* 6(5):677–698
- Reason, CJC, Landman W, Tennant W (2006) Seasonal to decadal prediction of southern African climate and its links with variability of the Atlantic Ocean. *Bull Am Meteorol Soc* 87(7):941–956
- Rind D, Goldberg R, Hansen J, Rosenzweig C, Ruedy R (1990) Potential evapotranspiration and the likelihood of future drought. *J Geophys Res-Atmos* 95(D7):9983–10004
- Rogelj J, Den Elzen M, Höhne N, Fransen T, Fekete H, Winkler H, Schaeffer R, Sha F, Riahi K, Meinshausen M (2016) Paris agreement climate proposals need a boost to keep warming well below 2 C. *Nature* 534(7609):631–639
- Scheff J, Frierson DM (2014) Scaling potential evapotranspiration with greenhouse warming. *J Clim* 27(4):1539–1558
- Schleussner CF, Rogelj J, Schaeffer M, Lissner T, Licker R, Fischer EM, Knutti R, Levermann A, Frieler K, Hare W (2016) Science and policy characteristics of the Paris agreement temperature goal. *Nat Clim Chang* 6(9):827–835
- Seibert M, Merz B, Apel H (2017) Seasonal forecasting of hydrological drought in the Limpopo Basin: a comparison of statistical methods. *Hydrol Earth Syst Sci* 21(3):1611–1629
- Skupin A, Agarwal P (2008) Introduction: What is a self-organizing map?. *Self-Organising Maps: Applications in Geographic Information Science*:1–20
- Spalding-Fecher R, Chapman A, Yamba F, Walimwipi H, Kling H, Tembo B, Nyambe I, Cuamba B (2016) The vulnerability of hydro-power production in the Zambezi River basin to the impacts of climate change and irrigation development. *Mitig Adapt Strateg Glob Chang* 21(5):721–742
- Thiemig V, Rojas R, Zambrano-Bigiarini M, Levizzani V, De Roo A (2012) Validation of satellite-based precipitation products over sparsely gauged African river basins. *J Hydrometeorol* 13(6):1760–1783
- Thornthwaite CW (1948) An approach toward a rational classification of climate. *Geogr Rev* 38:55–94
- Trambauer P, Werner M, Winsemius HC, Maskey S, Dutra E, Uhlenbrook S (2015) Hydrological drought forecasting and skill assessment for the Limpopo River basin, Southern Africa. *Hydrol Earth Syst Sci* 19(4):1695–1711
- Ujeneza EL, Abiodun BJ (2015) Drought regimes in Southern Africa and how well GCMs simulate them. *Clim Dyn* 44(5–6):1595–1609
- Vicente-Serrano SM, Beguería S, López-Moreno JI (2010) A multiscalar drought index sensitive to global warming: the standardized precipitation evapotranspiration index. *J Clim* 23(7):1696–1718
- Vicente-Serrano SM, Beguería S, López-Moreno JI (2010a) A multiscalar drought index sensitive to global warming: the Standardized Precipitation Evapotranspiration Index. *J Clim* 23:1696–1718
- Washington R, James R, Pearce H, Pokam WM, Moufouma-Okia W (2013) Congo Basin rainfall climatology: can we believe the climate models? *Philos Trans R Soc B* 368(1625):20120296
- Wehrens R (2011) *Chemometrics with R: multivariate data analysis in the natural sciences and life sciences*. Springer Science & Business Media, Berlin
- Yin J, He F, Xiong YJ, Qiu GY (2017) Effects of land use/land cover and climate changes on surface runoff in a semi-humid and semi-arid transition zone in northwest China. *Hydrol Earth Syst Sci* 21(1):183–196
- Zhang X, Zhang L, Zhao J, Rustomji P, Hairsine P (2008) Responses of streamflow to changes in climate and land use/cover in the Loess Plateau, China. *Water Resour Res* 44(7):W00A07
- Zhao T, Dai A (2015) The magnitude and causes of global drought changes in the twenty-first century under a low-moderate emissions scenario. *J Clim* 28(11):4490–4512